Raman spectroscopy on single- and multi-walled nanotubes under high pressure

C. Thomsen[1], **S. Reich**[1], **H. Jantoljak**[1], **I. Loa**[2], **K. Syassen**[2], **M. Burghard**[2], **G.S. Duesberg**[2], **S. Roth**[2]

[1] Institut für Festkörperphysik, Technische Universität Berlin, Hardenbergstrasse 36, D-10623 Berlin, Germany
[2] Max-Planck-Institut für Festkörperforschung, Heisenbergstrasse 1, D-70569 Stuttgart, Germany

Abstract. The pressure dependence of the high-energy Raman modes in single- and multi-walled carbon nanotubes was measured in the range 0–10 GPa. We found the pressure coefficient to be linear in both materials but 25% smaller in MWNT. Given that the curvature effects on vibrational properties of the rolled-up graphene sheets are small, we can explain this difference simply with elasticity theory.

PACS: 61.48.+c; 63.22.+m; 78.30.Na

The elastic properties of carbon nanotubes have become of scientific interest since it was recognized that the low atomic weight of carbon combined with a strong covalent bond has a high potential for a large-tensile-strength material [1, 2]. The graphene sheets allow for tube-like objects, which come in two different varieties: single- (SWNT) and multi-walled (MWNT) nanotubes. Single-walled nanotubes are formed by rolling up a single graphite sheet [3, 4]; several such tubes usually form a nanorope held together in a hexagonal lattice by van der Waals forces similar to the way plane graphene sheets are held together in graphite [5]. Multi-walled tubes consist of concentric graphene cylinders with increasing diameter [6]. The distance between two sheets is 3.4 Å, similar to the c-axis lattice constant of graphite [7, 8]. The size of a SWNT and the number of sheets in MWNT is determined by the preparation procedures, see for example [9, 10].

There have been various approaches to describe the elastic and vibrational properties of SWNT theoretically. They are based on force constants either taken from a fit to the full phonon dispersion curves of graphite and subsequent zone folding [11–13] or derived from ab initio pseudopotential calculations [14, 15]. One generally accepted conclusion of these various approaches is that the influence of the curvature on the elastic and vibrational properties is small: zone-folding methods ignore them completely whereas the ab inito calculations take them into account properly. Yet the calculated vibrational frequencies, except for for the narrower tubes, are similar [14]. The static elastic properties of nanoropes of

SWNT were calculated by Tersoff and Ruoff [16]. They predict the lattice constant of such a hexagonal lattice and its bulk modulus as a function of nanotube radius and pressure. MWNT have been too complicated in structure to allow for a calculation of their vibrational energies; their elastic properties were derived in [14] and [17].

Optical spectroscopy, in particular Raman spectroscopy, has been employed to study the vibrational properties of nanotubes experimentally. Single-walled nanotubes were found to have a series of peaks which may be grouped into modes around $150–200\,\mathrm{cm}^{-1}$ and a set just below $1600\,\mathrm{cm}^{-1}$. The low-energy modes are commonly considered to originate from radial breathing modes [18, 20–22] although a significant component resulting from tube–tube interactions in nanoropes is thought to be present [23, 24]. The high-energy modes correspond to carbon stretching vibrations similar to the high-energy modes in C_{60} and in graphite [25]. Based on group-theoretical considerations and lattice dynamical calculations A_{1g}, E_{1g}, and E_{2g} mode symmetries should be present among the high-energy peaks [14, 18, 19]. Infrared-active modes of SWNT were determined at 874 and $1598\,\mathrm{cm}^{-1}$ [26]. In multi-walled tubes there is only one high-energy Raman mode at $1583\,\mathrm{cm}^{-1}$ and a weak mode reminiscent of the so-called D-mode, a defect-induced mode, in graphite [7, 25, 27, 28].

1 Results

We report here the pressure dependence of the high-energy Raman modes in SWNT and MWNT. We find that whereas the dominant peak in the single-walled material has a pressure coefficient of $5.7\,\mathrm{cm}^{-1}/\mathrm{GPa}$, the corresponding peak of the multi-walled nanotubes shifts only with $4.25\,\mathrm{cm}^{-1}/\mathrm{GPa}$. Considering a nanotube as a hollow cylinder with a wall made of a mechanically isotropic medium, we show that the differences in pressure derivatives can be understood on the basis of elasticity theory.

The single- and multi-walled carbon nanotubes used in the present study were arc-discharge-grown samples prepared with a metallic catalyst (4.2% Ni and 1.0% Y). The

SWNT ropes contained about 20 nanotubes each [29]. The multi-walled sample was purified by applying size-exclusion chromatography [30]. Small flakes of the nanotube material were put into a gasketed diamond-anvil cell [31]. Using a 4 : 1 methanol–ethanol mixture as pressure medium we obtained pressures up to 10 GPa as determined by the ruby-luminescence method. The Raman spectra were recorded with a SPEX triplemate equipped with a charge-coupled device (CCD) detector. The 514 line of an Ar^+ laser was used for excitation; the spectral resolution was 3 cm^{-1}.

In Figs. 1 and 2 we display the high-energy part of the Raman spectrum of single-walled and multi-walled nanotubes, respectively, for various pressures. The figures show the decomposition of the high-energy spectrum in SWNT into three peaks as commonly observed, while the broader peak in MWNT is adequately described by a single Lorentzian. We see that the modes of the SWNT shift without changing the shape of the group of modes noticeably, i.e., all components have similar pressure coefficients. In Fig. 3 we show that the SWNT peaks vary linearly with pressure, with coefficients of 5.7, 5.8, and 5.8 cm^{-1}/GPa for the modes at 1593, 1569, and 1557 cm^{-1} (zero-pressure frequencies), respectively. The pressure dependence of the high-energy

Fig. 2. The high-energy mode of multi-walled nanotubes under various pressures. Only a single peak is resolved

mode of multi-walled nanotubes is shown in Fig. 3 for the same pressure range. We find that the peak in this material shifts also linearly but with a smaller pressure derivative of 4.25 cm^{-1}/GPa and a zero-pressure frequency of 1583 cm^{-1} (Fig. 3, Table 1).

In order to investigate the difference in pressure coefficients quantitatively, we derive the elastic properties of an individual nanotube (single- or multi-walled) under applied hydrostatic pressure. We approximate the nanotube by a hollow cylinder with a wall of finite thickness and closed ends. The wall which is rolled up to form the cylinder of a single-walled tube is thus assumed to have isotropic elastic properties. In view of the similarity of the vibrational and elastic

Fig. 1. Raman spectra in the high-energy range of single-walled carbon nanotubes for various hydrostatic pressures. Shown is the decomposition of the spectrum into three peaks, which are seen to shift with similar pressure coefficients
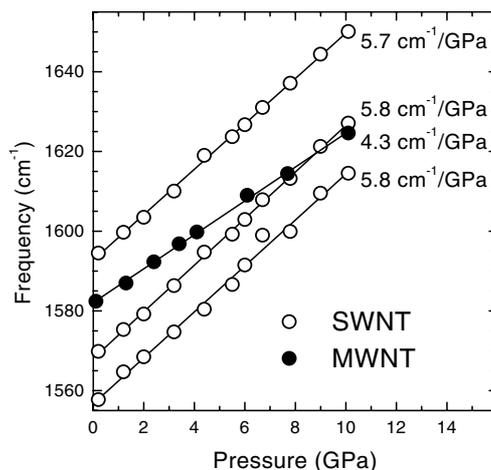
Fig. 3. Pressure slopes for the three modes in the high-energy range of SWNT and of the mode in MWNT. The latter is seen to be only 75% of that of SWNT

Table 1. Frequencies and logarithmic pressure derivatives for the high-energy modes of SWNT and MWNT. Data for graphite are listed for comparison

	$\omega_0/\mathrm{cm}^{-1}$	$\omega_0^{-1}\,\mathrm{d}\omega/\mathrm{d}p\,/\,\mathrm{TPa}^{-1}$
SWNT	1557	3.7
	1569	3.7
	1593	3.6
MWNT	1583	2.7
Graphite[a]	1579	2.96

[a] [32]

results of ab initio calculations compared to calculations not including curvature effects this approach is justified. Lu and Sánchez-Portal et al. have shown that the elastic properties of multi-walled tubes are not affected significantly by the van der Waals interactions between the sheets [14, 17]. We are thus able to determine strain components for both SWNT and MWNT in axial, tangential, and radial directions. *Tangential* in the following refers to a direction perpendicular to the axis and to the radius of the cylinder. We start from the equilibrium condition [33]

$$\frac{\partial \sigma_{ij}}{\partial x_k} = 0\,,$$

where σ_{ij} are the components of the stress tensor and x_k the normal variables. For the displacements u_i we obtain the condition

$$\mathrm{grad\ div}\ \mathbf{u} = 0 \tag{1}$$

since $\mathrm{rot}\ \mathbf{u} = 0$ in our problem, and we have used the following relation between stress und strain

$$\sigma_{ij} = \frac{E}{\nu^+}\left[\frac{\nu}{\nu^-}u_{ll}\,\delta_{ik} + u_{ik}\right]. \tag{2}$$

We use the abbreviations $\nu^+ = 1 + \nu$, $\nu^- = 1 - 2\nu$, $u_{ik} = 1/2\,(\partial u_i/\partial x_k + \partial u_k/\partial x_i)$, ν is Poisson's ratio, and E the Young's elastic modulus. As is conventional, repeated indices are to be summed over. From (1) we obtain

$$u_{rr} = a - \frac{b}{r^2}\,, \quad u_{\theta\theta} = a + \frac{b}{r^2}\,, \quad \mathrm{and} \quad u_{zz} = \mathrm{const}.$$

which may be inserted into (2) and, together with the boundary conditions for σ_{zz}, is used to evaluate a, b, and u_{zz}. The closed lid on the tubes leads to $\sigma_{zz} = -pA$ where $A = R_2^2/(R_2^2 - R_1^2)$ is the ratio of the total lid area to the area supported by the rim of the nanotube wall. Here, R_2 and R_1 are the outer and inner radii of the hollow cylinder, respectively. We thus obtain with $a = u_{zz} = -pA\,\nu^-/E$ and $b = -pA\,\nu^+ R_1^2/E$ the stresses in the two directions orthogonal to z:

$$\sigma_{rr} = -pA\left(1 - \frac{R_1^2}{r^2}\right) \quad \mathrm{and} \quad \sigma_{\theta\theta} = -pA\left(1 + \frac{R_1^2}{r^2}\right),$$

having assumed that the pressure at the tube wall from the outside is $-p$ and 0 on the inside. The corresponding strains are

$$u_{rr} = -\frac{pA\,\nu^-}{E}\left(1 - \frac{\nu^+}{\nu^-}\frac{R_1^2}{r^2}\right),$$

$$u_{\theta\theta} = -\frac{pA\,\nu^-}{E}\left(1 + \frac{\nu^+}{\nu^-}\frac{R_1^2}{r^2}\right), \quad \mathrm{and}$$

$$u_{zz} = -\frac{pA\,\nu^-}{E}\,. \tag{3}$$

The thus derived strain components of a hollow closed cylinder allow us to look at the nanotubes in the following way. Consider for a moment unwrapping the nanotube. We then have a single rectangular graphene sheet (SWNT) or a graphite-like stack of sheets (MWNT); one side of the rectangle has the circumference of the tube as its length, and applying pressure to the tube results in a strain along the axis (z) and in tangential direction (θ). If curvature effects are ignored, as in our model, the ratio of strains along the two sides of the rectangle is given by (3).

From this we are able to derive the ratio of pressure derivates for single- and multi-walled nanotubes. It is equal to the ratio of strains in the two types of tubes. From (3) we find

$$\frac{u_{zz}^{\mathrm{SW}}}{u_{zz}^{\mathrm{MW}}} = \frac{A^{\mathrm{SW}}}{A^{\mathrm{MW}}} \approx 1.5\,, \tag{4}$$

a result that assumes that the axial strain determines the pressure derivatives in Fig. 3, that ν and E are the same for SWNT and MWNT, and otherwise is of purely geometric nature. The inner and outer radii of our single-walled nanotubes were $R_1 = 5.2$ Å, $R_2 = 8.6$ Å (corresponding to a wall thickness of 3.4 Å), and Poisson's ratio $\nu = 0.14$ [14]. The outer radius ($R_2 = 75$ Å) of our MWNT we determined from a series of TEM pictures; the inner radius we took to be $R_1 = 20$ Å, a typical value [1, 34]. The experimental result (Fig. 3) is in agreement with (4): we find 1.35 for the ratio of pressure derivatives of the SWNT modes to the one of MWNT. We could have also taken the variation in circumference as dominanting the pressure derivatives with the same result. This follows for $u_{\theta\theta}^{\mathrm{SW}}/u_{\theta\theta}^{\mathrm{MW}}$ from (3) with $r = \sqrt{\nu^+/\nu^-}\,R_1$, the equilibrium radius of either single- or multi-walled tubes. The difference in pressure derivatives of the high-energy vibrations of single- and multi-walled nanotubes may hence be explained by the difference in wall thickness, which in turn determines how a hollow cylinder deforms under hydrostatically applied pressure.

2 Summary

We have shown that our results in single- and multi-walled carbon nanotubes may be explained by elasticity theory. The assumptions made – mechanically isotropic graphene sheets are rolled up to hollow cylinders and the eigenvectors of the high-energy Raman modes in SWNT and MWNT are similar – allow us to explain the ratio of pressure coefficients of these modes in single- and multi-walled nanotubes on geometrical grounds. Our results confirm that curvature effects on the vibrational and elastic properties of the graphene sheets are small.

References

1. M.M.J. Treacy, T.W. Ebbesen, J.M. Gibson: Nature (London) **381**, 678 (1996)
2. J.P. Salvetat et al.: Phys. Rev. Lett **82**, 944 (1999) and references therein
3. S. Iijima, T. Ichihashi: Nature (London) **363**, 603 (1993)
4. D.S. Bethune et al.: Nature (London) **363**, 605 (1993)
5. S. Bandow, S. Asaka, Y. Saito, A.M. Rab, L. Grigossian, E. Richter, P.C. Eklund: Phys. Rev. Lett. **80**, 3779 (1998)
6. S. Iijima: Nature (London) **354**, 56 (1991)
7. N. Chandrabhas et al.: Pramana J. Phys. **42**, 375 (1994)
8. Y. Saito, T. Yoshikawa, S. Bandow, M. Tomita, T. Hayashi: Phys. Rev. B **48**, 1907 (1993)
9. A. Fonseca et al., A.G. Rinzler et al.: Special issues on nanotubes, Appl. Phys. A **67**, 11, 29 (1998)
10. J.P. Salvetat, J.- M. Bonard, R. Bacsa, T. Stöckli, L. Forró: *Electronic Properties of Novel Materials – Progress in Molecular Nanostructures* ed. by H. Kuzmany, J. Fink, M. Mehring, S. Roth (American Institute of Physics, Woodbury 1998) p. 467
11. R.A. Jishi, L. Venkataraman, M.S. Dresselhaus, G. Dresselhaus: Chem. Phys. Lett. **209**, 77 (1993)
12. E. Richter, K.R. Subbaswamy: Phys. Rev. Lett. **79**, 2738 (1997)
13. A. Charlier, E. McRae, M.-F. Charlier, A. Spire, S. Forster: Phys. Rev. B **57**, 6689 (1998)
14. D. Sánchez-Portal, E. Artacho, J.M. Soler, A. Rubio, P. Ordejón: Phys. Rev. B **59**, 12678 (1999)
15. J. Kürti, G. Kresse, H. Kuzmany: Phys. Rev. B **58**, R8869 (1998)
16. J. Tersoff, R.S. Ruoff: Phys. Rev. Lett. **73**, 3336 (1994)
17. J.P. Lu: Phys. Rev. Lett. **79**, 1297 (1997)
18. A.M. Rao et al., Science **275**, 187 (1997)
19. M.S. Dresselhaus, G. Dresselhaus, P.C. Eklund: *Science of Fullerenes and Carbon Nanotubes* (Academic Press, New York 1996) p. 839
20. P.C. Ecklund, J.M. Holden, R.A. Jishi: Carbon **33**, 959 (1995)
21. E. Anglaret et al.: *Electronic Properties of Novel Materials – Progress in Molecular Nanostructures* ed. by H. Kuzmany, J. Fink, M. Mehring, S. Roth (American Institute of Physics, Woodbury 1998) p. 116
22. G.S. Duesberg, W. Blau, H.J. Byrne, J. Muster, M. Burghard, S. Roth: unpublished
23. C. Thomsen, S. Reich, A.R. Goñi, H. Jantoljak, P. Rafailov, I. Loa, K. Syassen, C. Journet, P. Bernier: Phys. Status Solidi B **215**, in print
24. U. Venkateswaran et al.: Phys. Rev. B **59**, 10928 (1999)
25. A. Kasuya et al.: Phys. Rev. Lett. **78**, 4434 (1997)
26. U. Kuhlmann, H. Jantoljak, N. Pfänder, P. Bernier, C. Journet, C. Thomsen: Chem. Phys. Lett. **294**, 237 (1998)
27. J. Kastner et al.: Chem. Phys. Lett. **221**, 53 (1994)
28. W.S. Basca, D. Ugarte, A. Châtelain, W.A. de Heer: Phys. Rev. B **50**, 15473 (1994)
29. C. Journet et al.: Nature **388**, 756 (1997)
30. G.S. Duesberg, M. Burghard, J. Muster, G. Philipp, S. Roth: Chem. Commun. **3**, 435 (1998)
31. G. Huber, K. Syassen, W.B. Holzapfel: Phys. Rev. B **15**, 5123 (1997)
32. M. Hanfland, H. Beister, K. Syassen: Phys. Rev. B **39**, 12598 (1989)
33. See, for example, Landau, Lifschitz: Vol. VII, *Elastizitätstheorie* (Akademie Verlag, Berlin 1991)
34. The numerical result in (4) actually does not depend much on the precise values for R_1 and R_2 of the MWNT as long as the outer radius is significantly larger than the inner one